Articles

Weak Protein−Protein Interactions Are Sufficient To Drive Assembly of Hepatitis B Virus Capsids†

Pablo Ceres and Adam Zlotnick*

Department of Biochemistry and Molecular Biology, University of Oklahoma Health Sciences Center, Oklahoma City, Oklahoma 73190

Received May 21, 2002; Revised Manuscript Received July 31, 2002

ABSTRACT: Hepatitis B virus (HBV) is an enveloped DNA virus with a spherical capsid (or core). The capsid is constructed from 120 copies of the homodimeric capsid protein arranged with $T = 4$ icosahedral symmetry. We examined in vitro assembly of purified *E. coli* expressed HBV capsid protein. After equilibration, concentrations of capsid and dimer were evaluated by size exclusion chromatography. The extent of assembly increased as temperature and ionic strength increased. The concentration dependence of capsid assembly conformed to the equilibrium expression: $K_{capsid} = [capsid]/[dimer]^{120}$. Given the known geometry for HBV capsids and dimers, the per capsid assembly energy was partitioned into energy per subunit−subunit contact. We were able to make three major conclusions. (i) Weak interactions (from −2.9 kcal/mol at 21 °C in low salt to −4.4 kcal/mol at 37 °C in high salt) at each intersubunit contact result in a globally stable capsid; weak intersubunit interactions may be the basis for the phenomenon of capsid breathing. (ii) HBV assembly is characterized by positive enthalpy and entropy. The reaction is entropy-driven, consistent with the largely hydrophobic contacts found in the crystal structure. (iii) Increasing NaCl concentration increases the magnitude of free energy, enthalpy, and entropy, as if ionic strength were increasing the amount of hydrophobic surface buried by assembly. This last point leads us to suggest that salt acts by inducing a conformational change in the dimer from an assembly-inactive form to an assembly-active form. This model of conformational change linked to assembly is consistent with immunological differences between dimer and capsid.

For many spherical viruses, the related reactions of capsid assembly and subsequent dissociation are central to the life cycle of the virus. The capsid must be stable enough to yield a structure that will survive between hosts. Paradoxically, for many viruses, such as hepatitis B virus (HBV)[1] *(1, 2)*, the capsid must dissociate to release its nucleic acid and infect the next host. Understanding capsid assembly and stability are critical to understanding virus function.

HBV is an enveloped DNA virus with an icosahedral capsid, or core. In vivo, the capsid protein assembles around a complex of viral RNA−reverse transcriptase *(3)* and host proteins *(4, 5)*. After assembly, the RNA pregenome is reverse-transcribed in situ. Later, the virus acquires its envelope and is secreted via the endoplasmic reticulum *(6, 7)*. Most capsids appear to have $T = 4$ quasi-symmetry (240 subunits), though a fraction forms smaller $T = 3$ particles *(8, 9)*. A second form of the capsid protein, which includes 10 additional N-terminal residues but lacks the 34 residue C-terminal RNA-binding domain, is secreted as a dimer. The secreted dimer, the e antigen (HBeAg), stimulates a distinctly different set of antibodies than the capsid (HBcAg). Some 'c' and 'e' epitopes map to the same sequence, but selective antibodies do not cross-react, suggesting a conformational difference. The difference in antigenicity correlates with particle assembly *(10)*.

We study the in vitro assembly of empty HBV capsids as a first approximation of virus assembly. The full-length capsid protein has 183 residues. However, the first 149 residues, lacking the C-terminal RNA-binding domain, form an assembly domain that spontaneously assembles when expressed in *E. coli (11)*. The truncated form of the capsid protein is dimeric, $Cp149_2$, and can be isolated and reassembled in response to high ionic strength and protein concentration *(10, 12−15)*. Capsid protein is dimeric; folded monomers have not been isolated [see Figure 1 and reference *(13)*]. The reassembled particles are >95% $T = 4$ *(14)*. Reconstructions of *E. coli* expressed capsids and reassembled particles *(14, 16, 17)* are essentially identical to those from in vivo sources *(9)*. High-resolution cryo-EM image recon-

† This work was supported by American Cancer Society Research Project Grant RPG-99-339-01 to A.Z.

* Correspondence should be addressed to this author at the Department of Biochemistry and Molecular Biology, University of Oklahoma Health Sciences Center, P.O. Box 26901, BRC464, Oklahoma City, OK 73190. Tel: (405) 271-9030; fax: (405) 271-3910; e-mail: adam-zlotnick@ouhsc.edu.

[1] Abbreviations: HBV, hepatitis B virus; SEC, size exclusion chromatography; MALLS, multi-angle laser light scattering; ASA, accessible surface area.

10.1021/bi0261645 CCC: $22.00
Published on Web 08/30/2002

structions *(18, 19)* and a crystal structure *(20)* of the $T = 4$ capsid suggest that the dimeric subunit is stabilized by a large four-helix bundle that forms protruding spikes over the capsid surface. The interdimer contacts are much smaller. The contact between each pair of dimers is isolated from other contacts. The observed geometry is consistent with describing the $T = 4$ capsid as a complex of 120 copies of tetravalent $Cp149_2$.

We have developed a description of capsid assembly that is based on fundamental thermodynamic and kinetic principles *(15, 21, 22)*. This model describes assembly as a cascade of low-order reactions. The basic model can be modified to include features such as nucleation. Using kinetic simulations, we found that assembly reactions closely approach equilibrium; they do not stall or become kinetically trapped except under extreme conditions *(22)*. Conversely, simulations of dissociation display a marked hysteresis (Singh and Zlotnick, unpublished results).

In this paper, we determine the thermodynamic parameters of HBV capsid protein self-association using data from assembly reactions. For the first time to our knowledge, we are able to dissect pairwise energetics for a spherical virus. Our experimental results were in qualitative agreement with the thermodynamic terms estimated from the crystal structure of the $T = 4$ capsid. We observed that the association energy becomes progressively stronger in increasing concentrations of NaCl, approaching the values calculated from the structure. We hypothesize that the effect of high salt is to induce the capsid protein to adopt an assembly-active conformation.

MATERIALS AND METHODS

Proteins. A 149 residue form of HBV capsid protein, lacking the C-terminal RNA-binding domain, was expressed in *E. coli*. The dimeric protein, $Cp149_2$, was purified as previously described *(23)*. The concentration of $Cp149_2$ was quantified by absorbance using $\epsilon_{280} = 60\,900\ M^{-1}\ cm^{-1}$.

Assembly Reactions. Prior to assembly, $Cp149_2$ was dialyzed into assembly buffer, 50 mM HEPES, pH 7.5, 1 mM DTT. Different dimer concentrations (1−25 μM) were assembled by mixing with an equal volume of high-salt assembly buffer to final NaCl concentrations of 0.15, 0.3, 0.5, and 0.7 M. Protein solutions and buffer were preequilibrated to reaction temperatures (17−41 °C) before initiating assembly.

After incubation, capsid and dimer concentrations were determined by size exclusion chromatography (SEC). Samples (50 μL) were injected onto a 28 mL Sephacryl S-300 HR column or a 21 mL Superose 6 column (Amersham-Pharmacia Biotech, Piscataway, NJ), connected to an AKTA-FPLC. Peaks were observed by absorbance at 280 nm and integrated using Unicorn software. Typically, reactions were about 80% complete in 1 h and reached equilibrium by 24 h.

Multi-angle laser light scattering analysis of SEC (MALLS-SEC) was performed using a Superose 6 column in line with a Dawn 17 angle MALLS detector and a DSP refractometer (both from Wyatt Technology, Santa Barbara, CA). Debye analysis of the data was performed using the program ASTRA (also Wyatt), assuming a refractive index increment of 1.85 for protein.

Data Analysis. The data obtained by SEC were analyzed to determine thermodynamic parameters. The reaction for capsid formation is represented in eq 1:

$$120\ \text{dimer} \Leftrightarrow \text{capsid} \tag{1}$$

From eq 1, an equilibrium expression can be derived:

$$K_{\text{capsid}} = [\text{capsid}]/[\text{dimer}]^{120} \tag{2}$$

The logarithmic form of eq 2 was used for actual calculation of K_{capsid} *(23)*. The units for K_{capsid} are M^{-119}, units which are difficult to interpret. However, given the capsid geometry, where 120 tetravalent subunits form 240 intersubunit contacts, K_{capsid} can be related to the bimolecular K_{contact} by eq 3, as previously shown *(22, 24)*.

$$K_{\text{capsid}} = \Pi_j s_i K_{\text{contact}}^{\ 240} \tag{3}$$

The term $\Pi_j s_i$ is a statistical term that describes the degeneracy of association based on capsid geometry. The value of $\Pi_j s_i$ for $T = 4$ HBV is $2^{119}/120$, so that $\ln(\Pi_j s_i)$ is 77.7. K_{capsid} can be related to another practical value, the apparent dissociation constant, $K_{\text{D,apparent}}$ (eq 4), where there are equal concentrations of reactant and product *(21, 22)*.

$$K_{\text{D,apparent}} = K_{\text{capsid}}^{\ (1/(-119))} \tag{4}$$

K_{contact} is also related to the free energy per contact of each dimer (eq 5):

$$\Delta G_{\text{contact}} = -RT \ln(K_{\text{contact}}) \tag{5}$$

where R is the gas constant and T is the temperature in degrees kelvin.

Calculation of Thermodynamic Parameters from Structural Data. Values for ΔG, ΔH, ΔS, and ΔC_p of association were calculated from the crystal structure of the $T = 4$ capsid *(20)* by the method of Baker and Murphy *(25)*. This empirical method is based on evaluating the change in the polar and nonpolar accessible surface areas, ΔASA_p and ΔASA_{np}, respectively. Briefly, ΔASA_p and ΔASA_{np} were calculated for free dimer and different quasi-equivalent contacts using the rolling probe algorithm *(26)* as implemented in the program NACCESS *(27)*. The probe size was the 1.4 Å diameter "water molecule", as suggested *(25)*. The change in surface area was used to calculate ΔH and ΔC_p. Entropy was partitioned into three components. The first, solvation entropy, was ΔASA-dependent. The second component describes immobilization of each amino acid side chain that becomes buried. The third component accounts for the loss of molecular rotational and translational entropy due to association of subunits into a larger assembly. In the Baker and Murphy algorithm, loss of rotational and translational entropy is parametrized for a value of -8 cal mol^{-1} deg^{-1}, which is in good agreement with experimental observations *(28−30)*. Though this value is equal to cratic entropy, the entropy for ideal mixing at standard state, the actual physical−chemical explanation and calculation of an entropy of mixing remain controversial [see *(30)* and references cited therein].

RESULTS

We evaluated assembly reactions with SEC (Figure 1A). SEC is a simple and direct method for determining concen-

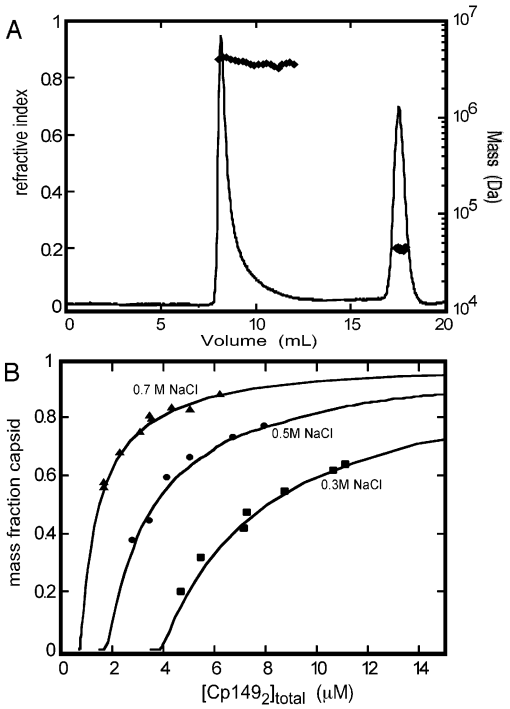

FIGURE 1: Analysis of $Cp149_2$ capsid assembly by size exclusion chromatography. (A) A typical assembly reaction of 15 μM $Cp149_2$ and 0.3 M NaCl resolved by SEC using a Superose-6 column 2 h after initiating assembly. Masses (diamonds) were determined by MALLS; the two major components were 4 MDa capsid and 35 kDa dimer. (B) Mass fraction of capsid formed as a function of total capsid protein in the reaction at 24 h. Reactions were performed at 25 °C with assembly induced by addition of 0.3 M (squares), 0.5 M (circles), and 0.7 M (triangles) NaCl. The solid curves are based on the equilibrium expression for capsid formation (eq 2).

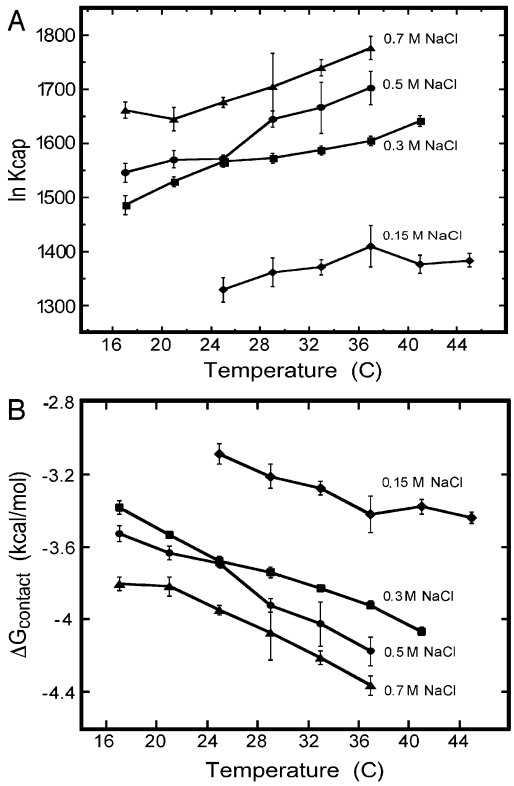

FIGURE 2: K_{capsid} and $K_{contact}$ vary as a function of temperature. (A) K_{capsid} is independent of $Cp149_2$ concentration, but sensitive to both NaCl concentration and temperature. The units for K_{capsid} are M^{-119}. (B) $\Delta G_{contact}$, derived from K_{capsid} (eq 3), becomes stronger as a function of ionic strength and temperature. Symbols are 0.15 M (diamonds), 0.3 M (squares), 0.5 M (circles), and 0.7 M (triangles) NaCl. Error bars represent 1 standard deviation based on 7−9 measurements for each solution condition.

trations of capsid and subunit *(15)*. More than 96% of the recovered mass was in capsid and dimer peaks. The capsid peak, eluting at 8 mL from a Superose-6 column, was asymmetric. MALLS mass determination showed that this broad peak was homogeneous, with a single molecular mass of 3.7 ± 0.3 MDa. This molecular mass was in agreement with the value predicted for a mixture of 95% of 4 MDa $T = 4$ capsid and 5% of 3 MDa $T = 3$ capsid *(14)*. The symmetrical dimer peak eluted at about 17 mL. Typically, MALLS analysis of this peak yielded a molecular mass of 40 kDa. No monomer peak was observed. Only a small amount of material migrated between capsid and dimer peaks with an intermediate molecular mass, in agreement with theoretical predictions for an assembly reaction at equilibrium *(22, 24)*.

Using different $Cp149_2$ concentrations, we generated isotherm-like assembly curves (Figure 1B). K_{capsid} was evaluated for individual reactions and averaged. Theoretical curves based on average K_{capsid} were in excellent agreement with data. Note that we predict no assembly at low $Cp149_2$ concentrations. This pseudo-critical concentration is a natural consequence of the steep concentration dependence defined in eq 1. The pseudo-critical concentration approximates the concentration where equal molar concentrations of dimer and capsid coexist, which we refer to as $K_{D,apparent}$ *(22, 24)*. At concentrations above $K_{D,apparent}$, the concentration of dimer is nearly constant (eq 2); for this reason, we plot the mass fraction of capsid against total $Cp149_2$, rather than free dimer as seen in a typical isotherm.

K_{capsid} is independent of protein concentration but is sensitive to temperature and [NaCl] (Figure 2A). The rate of assembly also increased with temperature (not shown) and ionic strength *(31)*. An average of 7−9 measurements at different $Cp149_2$ concentrations were used to calculate each K_{capsid}; about 200 chromatograms were used to generate Figure 2A. All experiments used for the calculations described in this paper were given 24 h to approach equilibrium. Results were no different at longer incubations of 72 and 96 h (not shown). At high salt (0.7 M) and temperature (>29 °C), concentrations of free dimer were so low that they were approaching the limits of our ability to accurately measure them. Also, we cannot exclude the possibility that those high-salt reactions had not equilibrated, but were stalled due to depletion of free subunit *(22)*. Thus, the ΔH and ΔS may be low estimates for the 0.7 M NaCl reactions from 29 to 37 °C.

The equilibrium constant K_{capsid} is in units of M^{-119}, which is not easily compared to the equilibrium constants of other reactions. However, from K_{capsid} we extracted the association constant for individual intersubunit contacts, $K_{contact}$ (eq 2, Figure 2B). In this calculation, we have assumed that all 240 quasi-equivalent interdimer contacts (in 4 distinct classes) have the same value for $K_{contact}$ and association energies are additive.

The values for $K_{contact}$ were surprisingly weak. Though it increased as temperature and NaCl concentration increased, it varied over a relatively narrow range corresponding to per

Table 1: Thermodynamics of HBV Assembly at 25 °C Based on Experimental Data

	[NaCl], M				
per contact energy[a]	0.15	0.3	0.5	0.7	calculated[b]
ΔG (kcal/mol)	-3.1 ± 0.1	-3.7 ± 0.2	-3.7 ± 0.2	-4.0 ± 0.2	-8.5 ± 0.8
ΔH (kcal/mol)	$+2.0 \pm 1.0$	$+4.3 \pm 0.4$	$+6.1 \pm 0.8$	$+6.2 \pm 0.2$	$+9.4 \pm 2.6$
$T\Delta S$ (kcal/mol)	$+5.1 \pm 1.1$	$+8.0 \pm 0.6$	$+9.8 \pm 1.0$	$+10.1 \pm 0.4$	$+18 \pm 3.7$
ΔS [cal/(mol·deg)$^{-1}$]	$+17 \pm 3.7$	$+27 \pm 2.0$	$+33 \pm 3.3$	$+34 \pm 1.3$	$+60 \pm 12$
$K_{D,apparent}$	14 μM	1.9 μM	1.8 μM	0.77 μM	0.14 pM

[a] Free energy per contact (ΔG) was from Figure 2B, enthalpy (ΔH) from the van't Hoff plots in Figure 3A, and entropy from $\Delta G = \Delta H - T\Delta S$. [b] For calculated values, see Table 2.

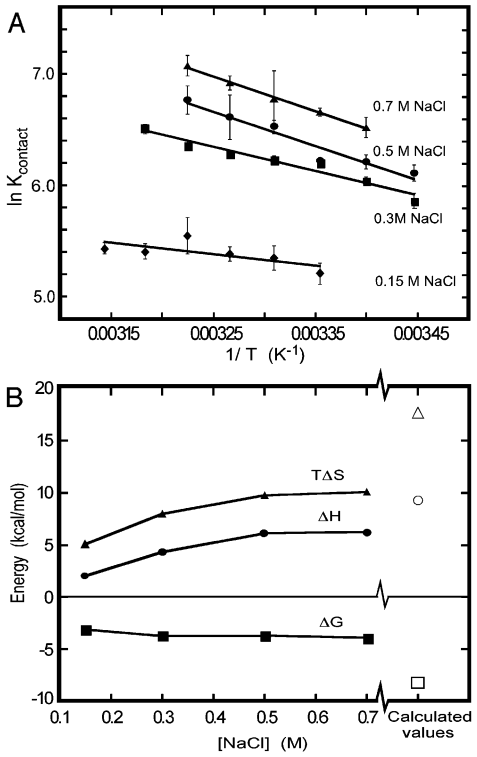

FIGURE 3: Thermodynamics of HBV capsid formation. (A) A van't Hoff plot shows the enthalpy of association is positive; the slope of the lines is equal to $-\Delta H/R$, where R is the gas constant. ΔH increases as NaCl concentration increases. NaCl concentrations are 0.15 M (diamonds), 0.3 M (squares), 0.5 M (circles), and 0.7 M (triangles). Error bars are 1 standard deviation calculated from at least 7 measurements. (B) The thermodynamic parameters for HBV capsid formation at 25 °C are shown as a function of [NaCl], $\Delta G_{contact}$ (squares), $\Delta H_{contact}$ (circles), and $T\Delta S_{contact}$ (triangles). Thermodynamic parameters, calculated from the structure *(25)* (open symbols), are in qualitative agreement with observed values.

contact dissociation constants from 0.75 to 7.8 mM. Small changes in $K_{contact}$ can be measured accurately because they cause a dramatic difference in stability due to the 240 contacts contributing to K_{capsid}. Viewed from a different perspective, the corresponding values for $K_{D,apparent}$, the pseudo-critical concentration of assembly, range from 0.7 to 15 μM [Table 1, eq 4; and see *(24)*].

Based on $K_{contact}$, we were able to describe the thermodynamic forces that affect HBV assembly. In a van't Hoff plot (Figure 3A), we relate the temperature dependence of $K_{contact}$ to enthalpy. The enthalpy of assembly is positive for all conditions that we examined. It became more positive with increasing NaCl concentration. We approximate enthalpy as a temperature-independent parameter because the data are insufficient to describe heat capacity-dependent curvature of the van't Hoff plots.

Table 2: Thermodynamic Parameters Calculated from the Capsid Structure (*25*)[a]

contact	ΔASA_p	ΔASA_{np}	ΔC_p	$\Delta H_{60°C}$	$\Delta H_{25°C}$	$\Delta S_{25°C}$	$\Delta G_{25°C}$
A−A	−306	−1040	−0.37	−1.35	+11.7	+68.1	−8.59
B−C	−324	−743	−0.25	−3.82	+5.05	+42.8	−7.70
D−B	−292	−931	−0.40	−1.75	+9.8	+59.6	−7.94
C−D	−378	−1140	−0.40	−2.74	+11.2	+69.9	−9.66
average	−325	−972	−0.36	−2.41	+9.43	+60.1	−8.47

[a] Units: ΔASA are in Å^2; ΔC_p and ΔS are in cal/(mol·deg)$^{-1}$; ΔH and ΔG are in kcal/mol. See the inset in Figure 4 for a description of interdimer contacts.

The positive $\Delta H_{contact}$ was compensated by a positive $\Delta S_{contact}$ (Figure 3B), calculated from $\Delta G = \Delta H - T\Delta S$. HBV capsid assembly is an entropy-driven reaction. Positive values for ΔH and ΔS are characteristic of reactions where there is a net loss of hydrophobic surface *(32−34)*.

Our experimental results qualitatively agree with the predictions based on structure (Tables 1 and 2). We examined each of the four unique interdimer contacts: A−A contacts at the icosahedral 5-fold and B−C, C−D, and D−B contacts around the quasi-6-fold vertex (Figure 4, inset). For this calculation, we made the simplifying assumption that AB and CD dimers as described in the crystal structure *(20)* are rigid bodies. Between 1100 and 1520 Å^2 of surface area is buried at interdimer contacts, resulting in a contact surface of 550−760 Å^2. The buried surfaces are about 75% hydrophobic, which is greater than the ~60% typical for a relatively small protein−protein interface *(35, 36)*. Consistent with burial of nonpolar surface, the calculated entropy and enthalpy were large and positive (Table 2) *(25)*; the heavily compensated free energy was relatively small and negative. Though the calculated enthalpy and entropy varied by 20% for the different interfaces, free energy varied by only 10% because of compensation.

The structure is not consistent with the observation that high salt increases association energy (Table 2, Figure 4). The intersubunit contact is stabilized by putative salt bridges, as well as hydrophobic surface. One would expect that increasing ionic strength should weaken salt bridges and have little effect on the strength of hydrophobic interactions *(32)*. This suggested that the role of high salt concentration might be to decrease water activity. However, when we examined the effect of a nonionic osmolyte [see *(37)* and references cited therein], we found that sucrose at concentrations of up to 1.2 M could not induce assembly of 10 μM $Cp149_2$ at 21 °C (not shown).

DISCUSSION

We have developed a protocol that allows evaluation of the thermodynamics of capsid formation in terms of indi-

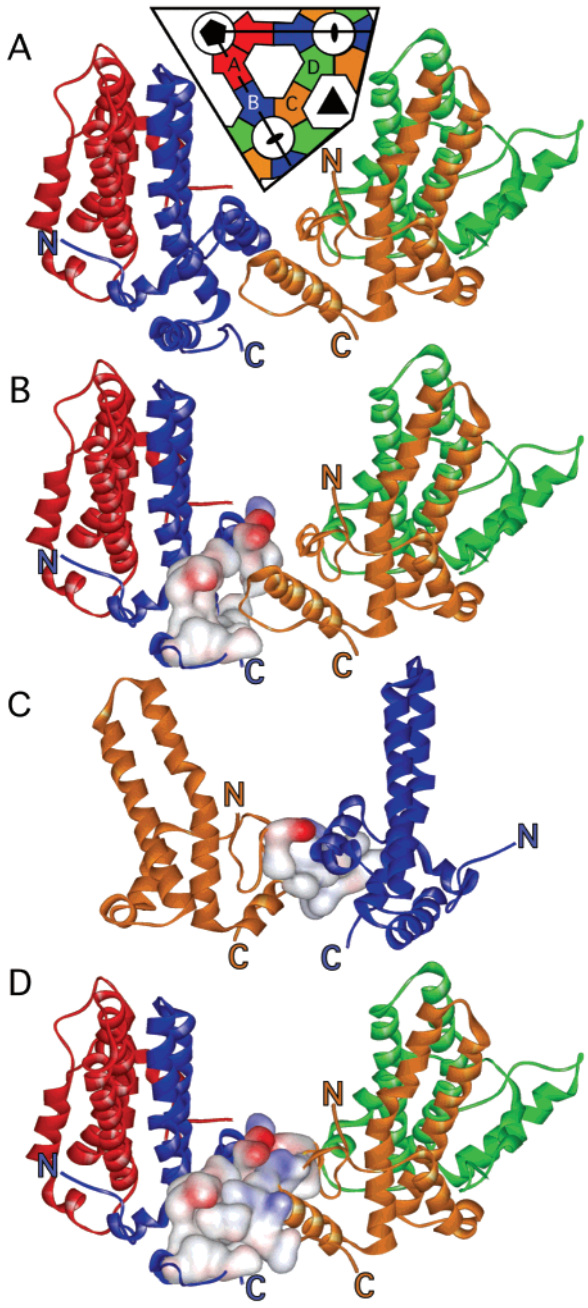

FIGURE 4: Representation of contact surfaces for the interdimer contact between B (blue) and C (orange) subunits. A map of the dimer−dimer interactions of a $T = 4$ capsid is shown in the inset. (A) A ribbon diagram shows that most contacts involve the N- and C-terminal helices and the C-terminal extended structure of both proteins. N- and C-termini are labeled for both subunits. Overall, the buried surface of the B−C contact is 71% is hydrophobic. (B) The surface of the C subunit is shown. Uncharged amino acids are colored white, acidic residues are red, and basic residues are blue. (C) The same diagram rotated 180° to show the complementary surface of the B subunit. The A (red) and D (green) subunits were removed for clarity. (D) Surfaces of both subunits show shape and charge complementarity. Coordinates are from the crystal structure *(20)*.

vidual subunit−subunit interactions. Making few assumptions, we are able to partition the overall association constant into the more readily understood bimolecular per contact energy. Our results with HBV show that a globally stable capsid can be the result of many weak intersubunit contacts. The temperature sensitivity of capsid assembly indicates positive enthalpy and entropy resulting in a negative free energy, hallmarks of association by burial of hydrophobic surface. The experimentally determined thermodynamic parameters qualitatively agree with calculations based on the capsid structure. We expect that this same approach will be applicable to other viruses. An important caveat is that HBV represents a structurally simple case because quasi-equivalence is so well maintained. In some other viruses, there are distinct differences between interfaces and there are more complex interactions involving several proteins [see *(38)*]. Nonetheless, it will be possible to calculate an average per subunit energy for any virus so long as there is an assembly reaction that will yield measurable quantities of capsid and subunit as it approaches equilibrium.

The peculiar geometry of HBV, where each intersubunit contact is well-defined and separate from others, facilitates comparison of experimental and calculated intersubunit contact energies. The experimental values are internally consistent and support our earlier prediction *(21)* that capsid assembly can be supported by a network of weak interactions. The experimental thermodynamic values were smaller than calculated values. This difference may be related to parametrization *(21)* or neglect of protein binding to NaCl. Alternatively, the difference may be due to a second energetic cost that is linked to the assembly reaction *(34, 39)*, i.e., folding or conformational change.

It is easy to conceptualize that locally weak interactions are the physical basis for the "breathing" that has been observed in the capsids of poliovirus *(40)*, Flockhouse virus *(41)*, and rhinovirus *(42)*, and also for the transient exposure of large epitopes appended to the C-terminus of Cp149 *(43)*. To breathe, capsids would transiently crack and re-form as individual contacts broke and, due to elevated local concentration, reassociated. Stronger association between subunits would reduce the frequency of breathing.

It may seem counterintuitive that entropy should be the driving force for organizing a regular structure. However, it is expected that when hydrophobic surfaces are buried, solvating water will be released, increasing the system entropy at a cost of a local decrease in entropy. There are many other examples of entropy-driven protein polymerization for fibers such as recA *(44)*, tubulin *(45)*, and collagen *(46)*. Entropy is also the driving force for assembly of rodlike tobacco mosaic virus *(47)*. Qualitatively, entropy was shown to be important for the stability of the spherical capsids of cowpea mosaic virus *(48)* and bacteriophage P22 *(49)*. The fraction of hydrophobic surface buried in HBV assembly may be atypically large compared to most protein−protein interfaces *(36)*; however, large hydrophobic contacts appear to be typical of virus capsids [see VIPER *(38)*], which suggests that entropy-driven capsid assembly may be a common feature of viruses.

Our data do not explain how ionic strength drives assembly. Increasing salt concentration increases the enthalpy and entropy of assembly (this report) as well as the rate of assembly *(31)*. Salt does not affect assembly by altering the activity of bulk water *(37)*. If it did, one would expect that a nonionic osmolyte such as sucrose would have at least as great an effect; yet, >1 M sucrose was incapable of inducing assembly. This suggests that assembly is induced because $Cp149_2$ binds NaCl, however weakly.

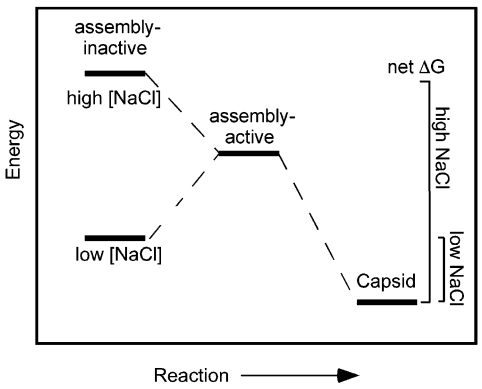

FIGURE 5: Hypothesis: assembly is activated by a conformational change that is induced by high ionic strength. Low ionic strength favors the assembly-inactive state, which corresponds to HBeAg. Dimers must undergo a conformational change prior to or concomitant with assembly, resulting in a weak net energy for capsid formation. In high ionic strength, the assembly-active state is favored, and the net energy for capsid formation is stronger. The energy for polymerization of the assembly-active form is about the same for both conditions.

We propose that high ionic strength activates assembly by inducing dimers to adopt an assembly-active conformation (Figure 5). At low ionic strength, where most $Cp149_2$ is in the assembly-inactive state, assembly is limited by the low concentration of active subunit and the energetic cost of converting it into an assembly-active form. At high ionic strength, most $Cp149_2$ is assembly-active; consequently, assembly results in a high yield of capsid.

Though we cannot exclude other mechanisms by which NaCl may drive assembly that are not obvious from the structure, our model is consistent with immunological evidence for a conformational difference between free dimer and dimer bound in capsid. Antibodies can be selective for free dimer (anti-HBeAg) or capsid (anti-HBcAg) despite binding to the same linear epitopes *(50)*. The process of capsid assembly and dissociation has been directly linked to differences in antibody reactivity *(10, 51)*. An image reconstruction shows that a capsid-specific Fab, which does not cross-react with free dimer, binds at the intradimer interface that is also presumably a feature of free dimer *(52)*. These results demonstrate an antigenic difference between dimer in the free (HBeAg-antigenicity) and capsid (HBcAg-antigenicity) forms that is most likely due to a conformational change within $Cp149_2$. A conformational transition as a prerequisite for assembly may not be unique to HBV; phage P22 capsid protein also shows evidence of conformational change concomitant with assembly *(49)*. An implication of our model of HBV assembly is that dimer structure will be distinct from capsid structure.

By quantifying assembly energy, this study helps to open the door for evaluating small molecules that interfere with HBV capsid assembly *(23)*. We have previously observed that bis-ANS binds to $Cp149_2$, but not capsid, and inhibits formation of normal capsids. Depending on conditions, assembly may be prevented or misdirected to yield noncapsid polymers. These new data suggest that bis-ANS may prefer to bind the assembly-inactive conformation.

This study of the assembly energetics of HBV has experimentally demonstrated that weak interactions drive capsid assembly and has provided new support for a second conformational state for the capsid protein, $Cp149_2$. The same techniques developed theoretically and applied to HBV can be used to determine the stability of other viruses and evaluate the effect of assembly mutants and inhibitors.

ACKNOWLEDGMENT

We thank Kenneth Murphy, Stephen Stray, Sushmita Singh, and Jennifer Johnson for comments and many helpful discussions.

REFERENCES

1. Guidotti, L. G., Martinez, V., Loh, Y. T., Rogler, C. E., and Chisari, F. V. (1994) Hepatitis B virus nucleocapsid particles do not cross the hepatocyte nuclear membrane in transgenic mice. *J. Virol. 68*, 5469−5475.
2. Kann, M., Sodeik, B., Vlachou, A., Gerlich, W. H., and Helenius, A. (1999) Phosphorylation-dependent binding of hepatitis B virus core particles to the nuclear pore complex. *J. Cell Biol. 145*, 45−55.
3. Bartenschlager, R., and Schaller, H. (1992) Hepadnaviral assembly is initiated by polymerase binding to the encapsidation signal in the viral RNA genome. *EMBO J. 11*, 3413−3420.
4. Kann, M., and Gerlich, W. H. (1994) Effect of core protein phosphorylation by protein kinase C on encapsidation of RNA within core particles of hepatitis B virus. *J. Virol. 68*, 7993−8000.
5. Hu, J., Toft, D. O., and Seeger, C. (1997) Hepadnavirus assembly and reverse transcription require a multi-component chaperone complex which is incorporated into nucleocapsids. *EMBO J. 16*, 59−68.
6. Ganem, D. (1996) in *Fields Virology* (Fields, B. N., Knipe, D. M., Howley, P. M., Chanock, R. M., Melnick, J. L., Monath, T. P., Roizman, B., and Straus, S. E., Eds.) pp 2703−37, Lippincott−Raven Publishers, Philadelphia.
7. Seeger, C., and Mason, W. S. (2000) Hepatitis B virus biology. *Microbiol. Mol. Biol. Rev. 64*, 51−68.
8. Stannard, L. M., and Hodgkiss, M. (1979) Morphological irregularities in Dane particle cores. *J. Gen. Virol. 45*, 509−514.
9. Kenney, J. M., von Bonsdorff, C. H., Nassal, M., and Fuller, S. D. (1995) Evolutionary conservation in the hepatitis B virus core structure: comparison of human and duck cores. *Structure 3*, 1009−1019.
10. Seifer, M., Zhou, S., and Standring, D. N. (1993) A micromolar pool of antigenically distinct precursors is required to initiate cooperative assembly of hepatitis B virus capsids in *Xenopus* oocytes. *J. Virol. 67*, 249−257.
11. Cohen, B. J., and Richmond, J. E. (1982) Electron microscopy of hepatitis B core antigen synthesized in *E. coli*. *Nature 296*, 677−679.
12. Zhou, S., and Standring, D. N. (1992) Hepatitis B virus capsid particles are assembled from core-protein dimer precursors. *Proc. Natl. Acad. Sci. U.S.A. 89*, 10046−10050.
13. Wingfield, P. T., Stahl, S. J., Williams, R. W., and Steven, A. C. (1995) Hepatitis core antigen produced in *Escherichia coli*: subunit composition, conformational analysis, and in vitro capsid assembly. *Biochemistry 34*, 4919−4932.
14. Zlotnick, A., Cheng, N., Conway, J. F., Booy, F. P., Steven, A. C., Stahl, S. J., and Wingfield, P. T. (1996) Dimorphism of hepatitis B virus capsids is strongly influenced by the C-terminus of the capsid protein. *Biochemistry 35*, 7412−7421.
15. Zlotnick, A., Palmer, I., Stahl, S. J., Steven, A. C., and Wingfield, P. T. (1999) Separation and Crystallization of $T=3$ and $T=4$ Icosahedral Complexes of the Hepatitis B Virus Core Protein. *Acta Crystallogr., D 55*, 717−720.
16. Crowther, R. A., Kiselev, N. A., Bottcher, B., Berriman, J. A., Borisova, G. P., Ose, V., and Pumpens, P. (1994) Three-dimensional structure of hepatitis B virus core particles determined by electron cryomicroscopy. *Cell 77*, 943−950.
17. Zlotnick, A., Cheng, N., Stahl, S. J., Conway, J. F., Steven, A. C., and Wingfield, P. T. (1997) Localization of the C terminus of the assembly domain of hepatitis B virus capsid protein: implications for morphogenesis and organization of encapsidated RNA. *Proc. Natl. Acad. Sci. U.S.A. 94*, 9556−9561.

18. Bottcher, B., Wynne, S. A., and Crowther, R. A. (1997) Determination of the fold of the core protein of hepatitis B virus by electron cryomicroscopy. *Nature 386*, 88−91.
19. Conway, J. F., Cheng, N., Zlotnick, A., Wingfield, P. T., Stahl, S. J., and Steven, A. C. (1997) Visualization of a 4-helix bundle in the hepatitis B virus capsid by cryo-electron microscopy. *Nature 386*, 91−94.
20. Wynne, S. A., Crowther, R. A., and Leslie, A. G. W. (1999) The Crystal Structure of the Human Hepatitis B Virus Capsid. *Mol. Cell 3*, 771−780.
21. Zlotnick, A., Reddy, V. S., Dasgupta, R., Schneemann, A., Ray, W. J., Jr., Rueckert, R. R., and Johnson, J. E. (1994) Capsid assembly in a family of animal viruses primes an autoproteolytic maturation that depends on a single aspartic acid residue. *J. Biol. Chem. 269*, 13680−13684.
22. Endres, D., and Zlotnick, A. (2002) Model-based Analysis of Assembly Kinetics for Virus Capsids or Other Spherical Polymers. *Biophys. J. 83*, 1217−1230.
23. Zlotnick, A., Ceres, P., Singh, S., and Johnson, J. M. (2002) A Small Molecule Misdirects Assembly of Hepatitis B Virus Capsids. *J. Virol. 76*, 4844−4848.
24. Zlotnick, A. (1994) To build a virus capsid. An equilibrium model of the self-assembly of polyhedral protein complexes. *J. Mol. Biol. 241*, 59−67.
25. Baker, B. M., and Murphy, K. P. (1998) Prediction of binding energetics from structure using empirical parametrization. *Methods Enzymol. 295*, 294−315.
26. Lee, B., and Richards, F. M. (1971) The interpretation of protein structures: estimation of static accessibility. *J. Mol. Biol. 55*, 379−400.
27. Hubbard, S. J., Campbell, S. F., and Thornton, J. M. (1991) Molecular recognition. Conformational analysis of limited proteolytic sites and serine proteinase protein inhibitors. *J. Mol. Biol. 220*, 507−530.
28. Murphy, K. P., Xie, D., Thompson, K. S., Amzel, L. M., and Freire, E. (1994) Entropy in biological binding processes: estimation of translational entropy loss. *Proteins: Struct., Funct., Genet. 18*, 63−67.
29. Tamura, A., and Privalov, P. L. (1997) The entropy cost of protein association. *J. Mol. Biol. 273*, 1048−1060.
30. Yu, Y. B. (2001) Standard state and thermodynamic self-consistency. *J. Pharm. Sci. 90*, 2099−2102.
31. Zlotnick, A., Johnson, J. M., Wingfield, P. W., Stahl, S. J., and Endres, D. (1999) A theoretical model successfully identifies features of hepatitis B virus capsid assembly. *Biochemistry 38*, 14644−14652.
32. Tanford, C. (1980) *The Hydrophobic Effect: Formation of Micelles and Biological Membranes*, 2nd ed., John Wiley and Sons, Inc., New York.
33. Baker, B. M., and Murphy, K. P. (1997) Dissecting the energetics of a protein−protein interaction: the binding of ovomucoid third domain to elastase. *J. Mol. Biol. 268*, 557−569.
34. Ayala, Y. M., Vindigni, A., Nayal, M., Spolar, R. S., Record, M. T., Jr., and Di Cera, E. (1995) Thermodynamic investigation of hirudin binding to the slow and fast forms of thrombin: evidence for folding transitions in the inhibitor and protease coupled to binding. *J. Mol. Biol. 253*, 787−798.
35. Miller, S., Lesk, A. M., Janin, J., and Chothia, C. (1987) The accessible surface area and stability of oligomeric proteins. *Nature 328*, 834−836.
36. Tsai, C. J., Lin, S. L., Wolfson, H. J., and Nussinov, R. (1997) Studies of protein−protein interfaces: a statistical analysis of the hydrophobic effect. *Protein Sci. 6*, 53−64.
37. Bolen, D. W., and Baskakov, I. V. (2001) The osmophobic effect: natural selection of a thermodynamic force in protein folding. *J. Mol. Biol. 310*, 955−963.
38. Reddy, V. S., Natarajan, P., Okerberg, B., Li, K., Damodaran, K. V., Morton, R. T., Brooks, C. L., III, and Johnson, J. E. (2001) Virus Particle Explorer (VIPER), a website for virus capsid structures and their computational analyses. *J. Virol. 75*, 11943−11947.
39. Murphy, K. P., Freire, E., and Paterson, Y. (1995) Configurational effects in antibody−antigen interactions studied by microcalorimetry. *Proteins: Struct., Funct., Genet. 21*, 83−90.
40. Li, Q., Yafai, A. G., Lee, Y. M.-H., Hogle, J., and Chow, M. (1994) Poliovirus neutralization by antibodies to internal epitopes of VP4 and VP1 results from reversible exposure of these sequences at physiological temperature. *J. Virol. 68*, 3965−3970.
41. Bothner, B., Dong, X. F., Bibbs, L., Johnson, J. E., and Siuzdak, G. (1998) Evidence of viral capsid dynamics using limited proteolysis and mass spectrometry. *J. Biol. Chem. 273*, 673−676.
42. Lewis, J. K., Bothner, B., Smith, T. J., and Siuzdak, G. (1998) Antiviral agent blocks breathing of the common cold virus. *Proc. Natl. Acad. Sci. U.S.A. 95*, 6774−6778.
43. Pumpens, P., Borisova, G. P., Crowther, R. A., and Grens, E. (1995) Hepatitis B virus core particles as epitope carriers. *Intervirology 38*, 63−74.
44. Brenner, S. L., Zlotnick, A., and Stafford, W. F. D. (1990) RecA protein self-assembly. II. Analytical equilibrium ultracentrifugation studies of the entropy-driven self-association of RecA. *J. Mol. Biol. 216*, 949−964.
45. Vulevic, B., and Correia, J. J. (1997) Thermodynamic and structural analysis of microtubule assembly: the role of GTP hydrolysis. *Biophys. J. 72*, 1357−1375.
46. Parkinson, J., Kadler, K. E., and Brass, A. (1995) Simple physical model of collagen fibrillogenesis based on diffusion-limited aggregation. *J. Mol. Biol. 247*, 823−831.
47. Smith, C. E., and Lauffer, M. A. (1967) Polymerization−depolymerization of tobacco mosaic virus protein. 8. Light-scattering studies. *Biochemistry 6*, 2457−2464.
48. da Poian, A. T., Oliveira, A. C., and Silva, J. L. (1995) Cold denaturation of an icosahedral virus. The role of entropy in virus assembly. *Biochemistry 34*, 2672−2677.
49. Tuma, R., Tsuruta, H., Benevides, J. M., Prevelige, P. E., Jr., and Thomas, G. J., Jr. (2001) Characterization of subunit structural changes accompanying assembly of the bacteriophage P22 procapsid. *Biochemistry 40*, 665−674.
50. Salfeld, J., Pfaff, E., Noah, M., and Schaller, H. (1989) Antigenic determinants and functional domains in core antigen and e antigen from hepatitis B virus. *J. Virol. 63*, 798−808.
51. Seifer, M., and Standring, D. N. (1993) Stability governs the apparent expression of "particulate" hepatitis B e antigen by mutant hepatitis B virus core particles. *Virology 196*, 70−78.
52. Conway, J. F., Cheng, N., Zlotnick, A., Stahl, S. J., Wingfield, P. T., Belnap, D. M., Kanngiesser, U., Noah, M., and Steven, A. C. (1998) Hepatitis B virus capsid: localization of the putative immunodominant loop (residues 78 to 83) on the capsid surface, and implications for the distinction between c and e-antigens. *J. Mol. Biol. 279*, 1111−1121.

BI0261645